inorganics

MDPI

Article

Study on Physicochemical and Thermal Properties of Tetrabutylammonium-Based Cation Ionic Salts Induced by Al_2O_3 Additive for Thermal Energy Storage Application

Inge M. Sutjahja [1,*], Surjani Wonorahardjo [2] and Surjamanto Wonorahardjo [3]

[1] Department of Physics, Faculty of Mathematics and Natural Sciences, Institut Teknologi Bandung, Jl. Ganesha 10, Bandung 40132, Indonesia
[2] Department of Chemistry, Universitas Negeri Malang, Jl. Semarang 5, Malang 65145, Indonesia; surjani.wonorahardjo@um.ac.id
[3] School of Architecture, Planning and Policy Development, Institut Teknologi Bandung, Jl. Ganesha 10, Bandung 40132, Indonesia; titus@ar.itb.ac.id
* Correspondence: inge@fi.itb.ac.id

Received: 22 August 2020; Accepted: 16 September 2020; Published: 18 September 2020



Abstract: The physicochemical and thermal properties of tetrabutylammonium bromide (TBA-Br) and tetrabutylammonium hexafluorophosphate (TBA-PF_6), and their change with the addition of Al_2O_3, were investigated using infrared (IR) spectroscopy and by simultaneously conducting thermal thermogravimetric (TG) analysis and differential thermal analysis (DTA) to obtain the differential scanning calorimetry (DSC) thermogram. The change in the IR data is characterized by the growth of a large peak in the range of 3500 cm^{-1} and the reduction of peaks below 1000 cm^{-1} with the additive concentration. The decomposition temperature determined from the peak in the DTG curve is nearly constant for TBA-Br, and it decreases with the addition of Al_2O_3 for TBA-PF_6, although it does not depend on the concentration of the additives. The DTA curve of ionic salts with the addition of Al_2O_3 shows additional peaks, which indicates a change in the sample's temperature at disorder or phase transitions. The variation in the melting temperature with additive concentration is similar to that of decomposition temperature. The maximum heat of fusion value was approximately 67 kJ kg^{-1} for the doped TBA-Br and TBA-PF_6 but was achieved at a different additive concentration. This is due to the additional disorder in the system induced by the dissolution of Al_2O_3.

Keywords: tetrabutylamonium bromide; tetrabutylamonium hexafluorophosphate; aluminium oxide additive; infrared (IR); decomposition and melting temperature; heat of fusion

1. Introduction

Ionic salts are composed of organic cations and inorganic anions with relatively low melting points below approximately 100 °C. The liquid state of this material is commonly known as an ionic liquid (IL). For the last several years, ILs have been extensively investigated in many areas, such as catalysis, synthesis, extraction, and separation, owing to their common characteristics such as low vapour pressure, high thermal stability, low viscosity, large liquidus range, and favorable solvation behavior [1–3]. Additionally, the use of ILs in the field of thermal energy storage (TES) has also been investigated, and ILs have promising applications as liquid thermal storage media, heat-transfer fluids (HTFs) [4,5], and electrolytes in energy storage systems (supercapacitors, Li batteries, fuel cells, and dye-sensitized solar cells) [6–8]. Some types of ILs with high latent heat and a proper melting point, such as tetraalkylammonium [9] and alkylimidazolium [10,11] with relatively long-chain characteristics,

are also suitable as phase change materials (PCMs). For TES media or HTFs in solar energy storage, various basic investigations have been intensively conducted with regard to the thermodynamic properties of ILs, which include density, heat capacity, thermal conductivity, and latent heat of fusion.

Similar to common HTF or PCM, the physical and chemical properties of ionic salts or ILs are influenced by chemical additives. In 2007, Fukushima and Aida [12] conducted pioneering research by mixing a high concentration of carbon nanotubes (CNT) into ILs at room temperature to form gels known as bucky gels, which have potential applications in many engineering and chemical processes. This was adopted by de Castro et al. in 2010 [13], who reported for the first time the enhancement of thermal conductivity and heat capacity values for several ILs containing CNT. The behavior of these ionanofluids, which is not explained by existing theories, suggests that nanocluster formation and the preferred paths for heat and storage are present and likely responsible for the observed phenomena. It was further suggested and experimentally proven that the possibility of using ILs containing dispersed nanoparticles with specific functionalization, such as single-walled nanotubes, multi-walled nanotubes, graphene, and fullerenes (C_{60} and C_{80}, for example), opens the door to many potential applications [14–17].

Apart from carbon-based additives, Au, CuO, SiO_2, carbon-coated Ni, and Al_2O_3 nanoparticles have also been added to some ILs, and their thermophysical properties have been investigated [18–25]. A review of relevant research has been presented in [26]. The effects of the Al_2O_3 additive on the physical and chemical properties of ILs have been studied for ammonium $[N^+_{4111}][NTf_2]$, including the enhancement of thermal conductivity, viscosity, heat capacity, and heat transfer coefficient for 0.5 wt % additive [22]. The experimental data for imidazolium-based ILs generally show the increase in density, heat capacity and volumetric heat capacities, thermal conductivity, and viscosity with an increase in Al_2O_3 concentration up to 10 wt % for $[C_4mmim][NTf_2]$ [24] and up to 2.5 vol % for $[C_4mim][NTf_2]$ and $[C_4mpyrr]NTf_2]$ [26]. The superiority of Al_2O_3 compared with carbon black is also shown by a significant improvement in the thermal stability without the volatilization of IL [24] and the enhancement of heat transfer coefficient [26], which is an important parameter for evaluating the overall thermal performance. Bai et al. [25] reported that the supercooling of $[C_{16}MMIM]Br$ shows a decreasing trend for copper and graphite powder additives up to 10 wt % concentration and an increasing trend beyond that up to 25 wt % with a monotonous decrease of melting enthalpy. The results of this study show that there is an optimum condition of the additive content for the satisfactory performance of ionic salts in the TES system.

In this paper, we describe the role of the Al_2O_3 nanoparticle additive in the physicochemical and thermal properties of tetrabutylammonium bromide (TBA-Br) and tetrabutylammonium hexafluorophosphate (TBA-PF_6) ionic salts. The investigated properties include the transmittance of infrared spectra, melting and decomposition temperatures, and latent heat of fusion for the solid-liquid phase transition. Recently, Bhatt and Gohil [27] reported the performance of several ionic salts based on the tetrabutylammonium cation with varied inorganic anions as the TES material for a solar cooker application. They found that relatively simple types of anions (iodate IO_3, nitrate NO_3, bromide Br, and tetrafluoroborate BF_4) have higher efficiency than bulky anions (hexafluorophosphates PF_6, bromate BrO_3, and thiocyanate SCN). Al_2O_3 is an amphoteric oxide exhibiting strong adsorptive properties [28] and is typically used as an adsorbent. Additionally, it has more ionic properties and the intermolecular forces in the IL result in different IL features.

TBA-Br and TBA-PF_6 are quaternary ammonium salts consisting of positively charged (cation) tetrabutylammonium, and negatively charged (anion) bromide and hexafluorophosphate. As shown in Figure 1, they have similar structure: the ammonium cations form a tetrahedral structure and two linear C_8H_{18} organic chains are interconnected with each other through an inorganic N^+ ion. All bonds between the C and H atoms have the characteristics of a single covalent bond [29].

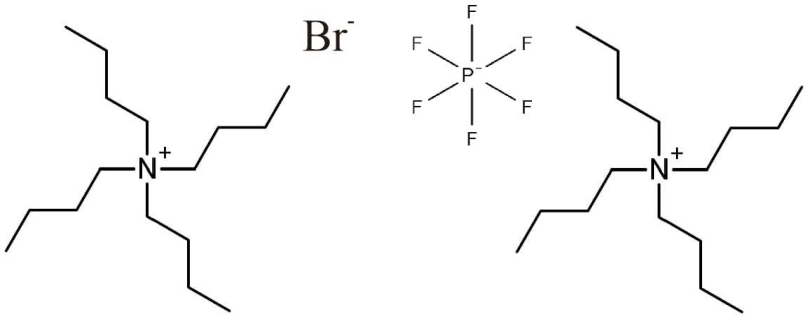

(**a**) (**b**)

Figure 1. Structure of (**a**) TBA-Br and (**b**) TBA-PF_6.

Amongst the homologous series of symmetric alkylammonium halides, the thermal properties of this tetrabutylammonium are categorized as intermediate alkyl-chain lengths. Specifically, this tetrabutylammonium undergoes a combination of orientational and conformational disordering, which allows for both the possibility of plastic and conformationally disordered (condis) crystals [30]. The assessment of disorder in this crystal structure is based on entropy investigations [30], and the disorder is clearly observable as a change in the local structure [29]. Hence, any loss of order is followed by the emergence of heat of fusion, and multiple step fusion is related to the mesophases, which are distinct from both the perfect (rigid) crystal and the isotropic melt. In previously reported studies, the melting temperatures of TBA-Br and TBA-PF_6 were reported as approximately 120 °C [9,29,30] and 240–250 °C [30,31], respectively.

For this symmetric alkylammonium, the cation and anion interaction and its charge transfer depend on the Coulomb interaction between the cation and anion by ionic bonding. Owing to the carbon position difference in the alkyl chain, the carbon directly bound to the nitrogen is expected to have the highest binding energy because it is closest to the electropositive nitrogen, followed by the next carbon atom along the chain and the remaining carbons [32]. However, the charge transfer may also depend on the type of anion. In this case, Br^- is classified as a halide anion with strong proton acceptors, while PF_6^- is classified as a weakly coordinated molecular anion [31,33–35]. The intermolecular interaction is dominated by the hydrogen bond owing to the existence of fluoride and nitrogen ions [32,36] in the same manner as in the case of the imidazolium-based IL [11]. Considering the larger negative charges of Br^- compared with PF_6^-, it is assumed that TBA-Br has larger heat of fusion values compared with TBA-PF_6 [11]. However, the phosphonium ion with six fluoride atoms would also be bulky and cause steric hindrance to the ammonium ion in the TBA-PF_6 rather than to the bromium ion in the TBA-Br, which would in turn make the molecule vulnerable [31]. In the presence of Al_2O_3, the ILs undergo new molecular interaction, which can be observed using IR spectroscopy and thermogravimetry.

2. Results and Discussion

2.1. IR Spectra

The IR spectra of the TBA-Br+Al_2O_3 (Figure 2) and TBA-PF_6+Al_2O_3 additive (Figure 3) ionic salts are presented (a) in the range of 400 to 2000 cm^{-1} and (b) 2000 to 4000 cm^{-1}. The figures also show the IR spectra for the Al_2O_3 additive.

For the pure TBA-Br and TBA-PF_6 samples, the peaks from 2850 to 3000 cm^{-1} originated from the asymmetric/symmetric stretching vibration of the C–H, –CH_2–, and –CH_3 groups, while the peaks from 1300 to 1470 cm^{-1} originated from the CH_2 and CH_3 asymmetric/symmetric bending vibration. The $(CH_2)_n$rocking for $n \geq 3$ is indicated by the peaks in the range of 750–720 cm^{-1}. The C–N bonding is revealed by the peaks at approximately 1000–1350 cm^{-1}. The region between 600 and 1400 cm^{-1} is

the fingerprint of the molecule, and is dominated by the C–C and C–N bonding in this case [37]. For the TBA-PF_6 sample, the symmetric stretching of the highly symmetric PF_6 anion is indicated by the peak at approximately 841 and 740 cm^{-1}, while the bending is indicated by the peak at 558 cm^{-1} [38].

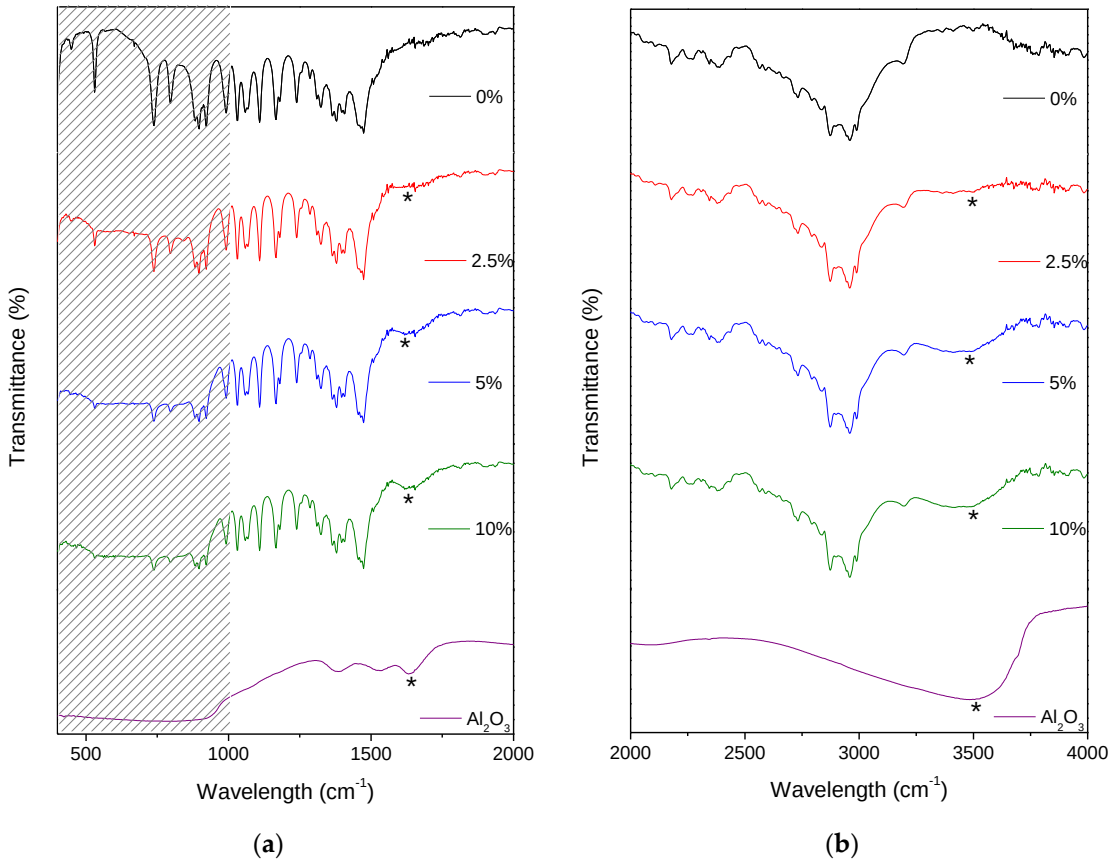

Figure 2. IR spectra obtained for TBA-Br+Al_2O_3 additive in range of (**a**) 400–2000 cm^{-1} and (**b**) 2000–4000 cm^{-1}, and the Al_2O_3 additive.

Upon addition with Al_2O_3, the overall peaks in the range of 1000 to 3250 cm^{-1} did not change with the increase of Al_2O_3 additive. This indicates that the alkyl groups, and both types of tetrabutyl groups, remained unchanged because all –C–H and –C–C– covalent bonds were sufficiently strong to maintain the molecules while Al_2O_3 was introduced. Two types of changes are clearly observable in the infrared spectra of both compounds: (i) the appearance of a broad peak at a high wavenumber of approximately 3500 cm^{-1} (asterisk in Figures 2b and 3b) and (ii) the disappearance of some peaks at a lower wavenumber below 1000 cm^{-1} (shaded region in Figures 2a and 3a).

There are some possibilities related to the growth of a broad peak at approximately 3500 cm^{-1} with the increase of transmittance intensity upon increasing the additive concentration. The first possibility is that water adsorbed on a metal oxide solid (OH stretching) [39]. This possibility is also shown by the peak at around 1630 cm^{-1} (OH bending) of TBA-Br salt with Al_2O_3 additive (asterisk in Figure 2a). The second possibility is the remaining Al_2O_3 nanoparticle [40], which raised the intensity according to the increased fraction in the composition.

The disappearance of the peaks below 1000 cm^{-1} becomes more pronounced with the increase of additive concentration, and is more pronounced for the TBA-Br sample compared with the TBA-PF_6 sample. Various explanations have been proposed for this phenomenon. The Lewis acid Al_2O_3 is assumed to dissolve in ionic salts [41], and its acidity weakens or disrupts the cation and anion interaction of the ionic salts [42]. Compared with its phosphonium counterpart, the steric effect is

more pronounced in this ammonium ionic salt, and, thus, the anion cannot approach the centre of the positive charge cation [43], likely resulting in weak cation–anion interactions [38].

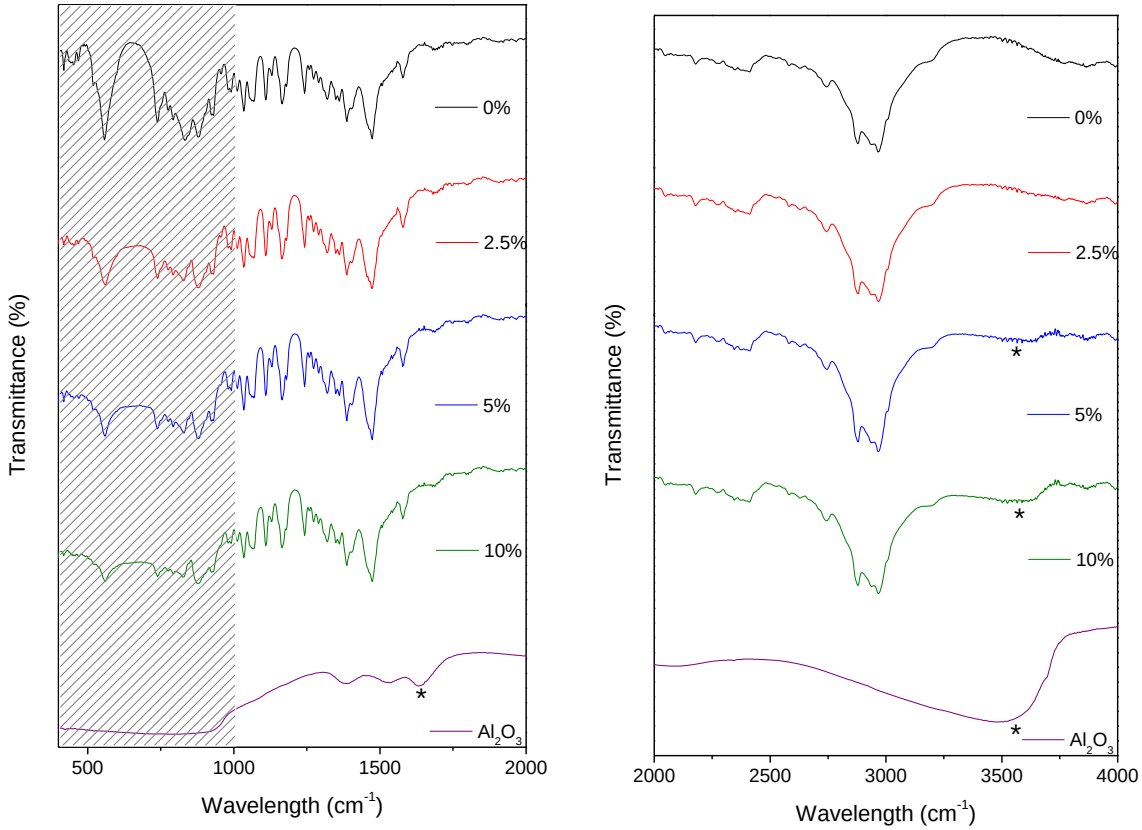

Figure 3. IR spectra obtained for TBA-PF_6+Al_2O_3 additive in range of (**a**) 400–2000 cm^{-1} and (**b**) 2000–4000 cm^{-1}, and the Al_2O_3 additive.

2.2. Thermal Properties

The thermal stability of a material is typically measured by the decomposition temperature (T_d). In the case of the TBA-Br and TBA-PF_6 ionic salts, their structure consists of a complex functional group instead of a simple alkyl chain. Thus, it is expected that the thermal stability will improve as the strength of the intermolecular interaction increases because there is more energy in the chemical bond. In other words, more energy will be absorbed when the chemical bonds are broken, which increases the T_d [44]. However, compared with the covalent bond, the ionic interaction can be spontaneously broken because of intermolecular forces. The addition of additive will make easy changes to the IL, as has already been observed in the IR spectra.

The thermal analysis curves of the functionalised ionic salts are presented in Figure 4 for the TBA-Br sample and in Figure 5 for the TBA-PF_6 sample. The graphs from (a) to (d) represent the curves for a pure sample with 2.5, 5, and 10 wt % of Al_2O_3 additive. Each graph shows the TG, differential TG (DTG), and DTA curve.

Overall, the TG curves of TBA-Br+Al_2O_3 ionic salts have a relatively constant value before suddenly decreasing owing to the change of the sample's mass. This sudden decrease in the TG curves is also reflected by the large and broad peak of the DTG curves. The DTA curves exhibit various peaks at low temperatures and an additional valley near the peak of the DTG curves for additive samples (red arrows in Figure 4), which indicates the change in the sample's temperature at disorder or phase transition.

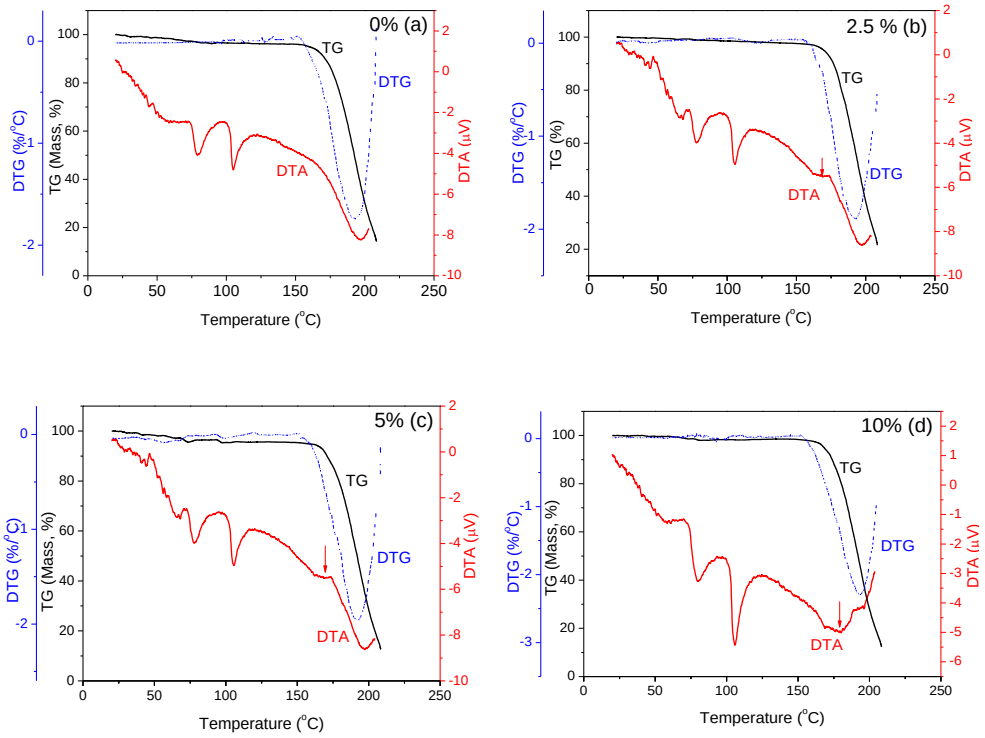

Figure 4. TG, DTG, and DTA curves of (**a**) TBA-Br with Al_2O_3 additive at concentration of (**b**) 2.5, (**c**) 5, and (**d**) 10 wt %.

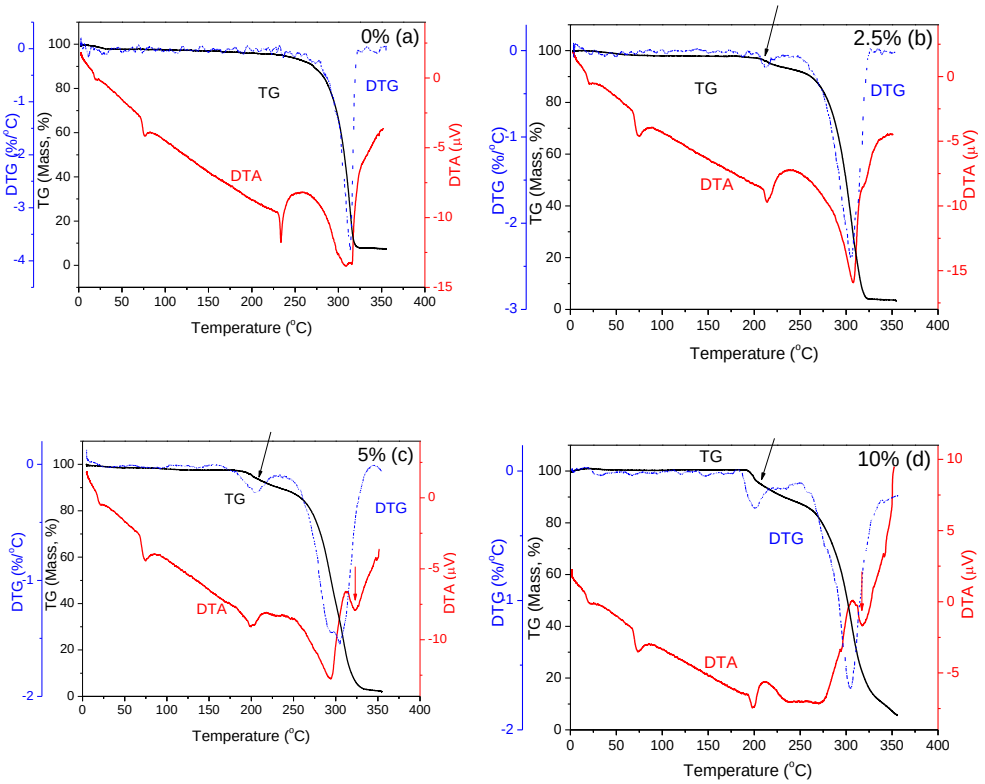

Figure 5. TG, DTG, and DTA curves of (**a**) TBA-PF_6 with Al_2O_3 additive at concentration of (**b**) 2.5, (**c**) 5, and (**d**) 10 wt %.

A closer look at the TG curves in Figure 5 reveals a difference near the sudden drop; namely, a shoulder for the TBA-PF_6 sample (black arrows in Figure 5), which becomes more pronounced as the Al_2O_3 additive concentration increases. The DTG curve of TBA-PF_6 with Al_2O_3 additive showed a double peak, where the low temperature peak is related to the shoulder in the TG curves and high-temperature peak is related to a sharp drop in the TG curves. The sample with 5 wt % additive concentration exhibited double peaks in close proximity with each other in the DTG curve, as indicated by the dotted line in Figure 5c. This behavior indicates that TBA-PF_6 sample and its additive compound decompose with an intermediate step, presumably owing to the bulky PF_6 anion. The shift to lower temperature of the high-temperature DTA peak near the large DTG peak might be due to the reaction between dissolved Al_2O_3 and the decomposition product of TBA-PF_6. According to Zhuravlev et al. [31], the decomposition of TBA-PF_6 is mainly determined by the decomposition of the cation, which may involve the formation of hydrofluoric acid gas and phosphorus pentafluoride. This might be related to the DTA data for the samples with high additive content (5 wt % and 10 wt %) that show an additional peak at a high temperature above the large peak of the DTG curve (red arrows in Figure 5).

The results for the variation in the decomposition temperature with the additive concentration, which were obtained using the peak in the DTG curve, are shown in Figure 6. For TBA-Br, the decomposition temperature was nearly constant, whereas for TBA-PF_6, the high-temperature decomposition temperature decreased with Al_2O_3 addition, although it did not depend on the concentration of the additives.

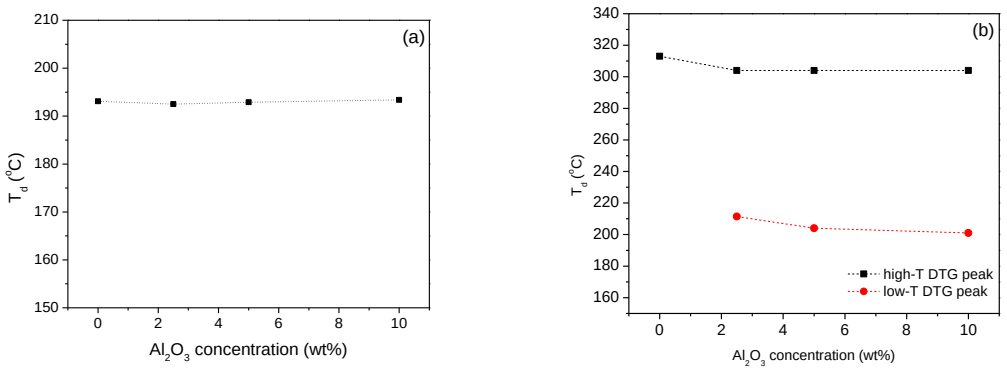

Figure 6. Decomposition temperature of (**a**) TBA-Br and (**b**) TBA-PF_6 with Al_2O_3 additive concentration.

The DSC thermograms of the TBA-Br and TBA-PF_6 samples shown in Figure 7a,b generally exhibit additional endothermic peaks prior to the melting point (T_m), owing to the disorder transition that occurs in the samples before melting [9,30,45]. Then, the melting endotherms are used to calculate the total heats of fusion (ΔH_m), as presented in Table 1. Notably, the peaks in these thermograms should be related to the DTA curves. However, indirect measurement has a hindering effect on the accuracy of the DSC data.

Table 1. Phase transition temperatures and melting enthalpy of TBA-Br+Al_2O_3 additive and TBA-PF_6+Al_2O_3 additive from DSC thermogram.

Al_2O_3/(wt %) [c]	TBA-Br [a] + Al_2O_3				TBA-PF_6 [b] + Al_2O_3			
	Phase Transition Temps. (°C) [d]			ΔH_m/ (kJ kg^{-1}) [f]	Phase Transition Temps. (°C) [d]			ΔH_m/ (kJ kg^{-1}) [f]
	1st Peak [e]	2nd Peak	3rd Peak		1st Peak	2nd Peak	3rd Peak	
0	58	93	119	45	~20 [e]	91	248	35
2.5	66	92	120	67	21	73	214	22
5	67	94	120	43	35	87	213	68
10	58	93	120	44	34	88	213	27

[a] Tetrabutylammonium bromide. [b] Tetrabutylammonium hexafluorophosphate. [c] additive concentration. [d] From the peaks in DSC thermogram. [e] From the DTA curve. [f] Total heats of fusion from DSC thermogram.

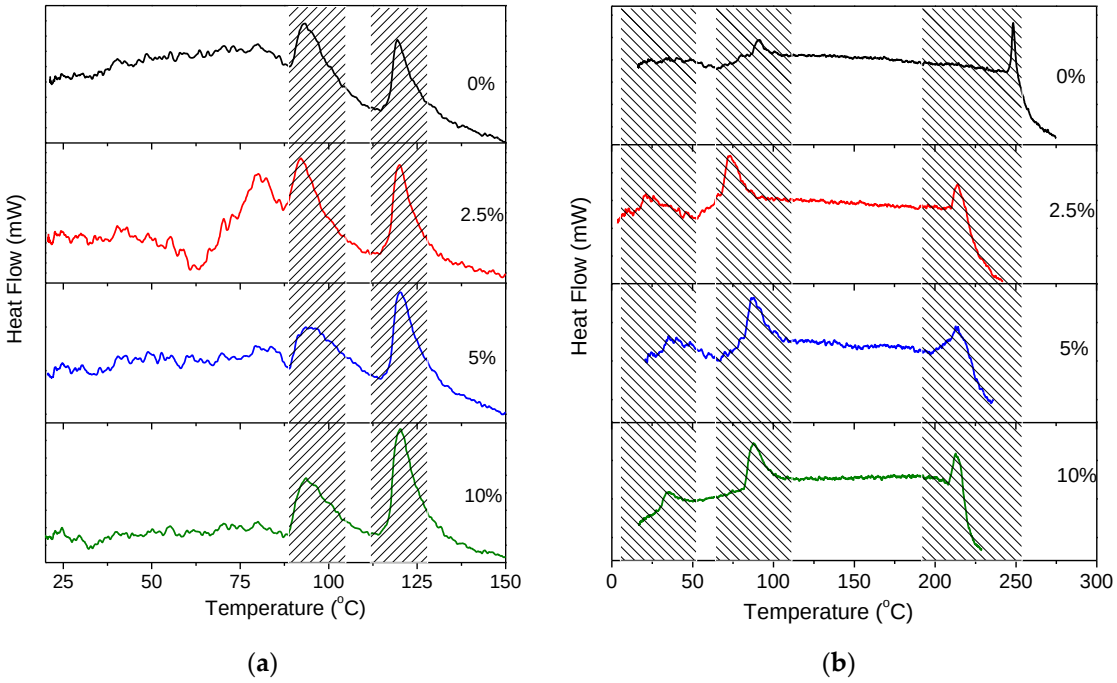

Figure 7. DSC thermogram of (**a**) TBA-Br+Al_2O_3 and (**b**) TBA-PF_6+Al_2O_3 at various Al_2O_3 concentration.

For the pure TBA-Br sample, the results revealed that the melting temperature is approximately 120 °C, which is in good agreement with the results reported by previous studies [9,29,30]. With regard to the intermediate alkyl-chain lengths, the low temperature transition (first peak, not clearly observed in Figure 7a) and the temperature of 93 °C are related to the crystal readjustment and conformational disorder of the crystal, while the high-temperature transition is related to the final isotropization [30]. The total heat of fusion was approximately 45 kJ kg^{-1}, which is in good agreement with the results reported by Burns and Verrall [9], but lower than that reported by Xenopoulos [30]. The T_m and ΔH_m results are largely different from those reported by Bhatt and Gohil [27]. Upon Al_2O_3 addition, the melting temperature was approximately constant. An additional peak at a temperature of approximately 80 °C (66 °C from the DTA curve) was clearly observable for an Al_2O_3 additive concentration of 2.5 wt % and resulted in the highest heat of fusion value, which was approximately 67 kJ kg^{-1}. The other samples may also have additional peaks at low temperatures (see the DTA curves in Figure 4), but these peaks are not obvious in this thermogram.

The results revealed that the melting temperature for pure TBA-PF_6 was approximately 248 °C, with a total heat of fusion of approximately 35 kJ kg^{-1}. These values are in fairly good agreement with those reported by previous studies [30,31], but are largely different from those reported by Bhatt and Gohil [27]. Upon Al_2O_3 addition, the melting temperature of TBA-PF_6 decreased and remained

relatively stable with an additive concentration of up to 10 wt %. The total heat of fusion had the highest value of approximately 68 kJ kg^{-1} for an Al_2O_3 additive concentration of 5 wt %.

The variation in melting temperatures for TBA-PF_6 and TBA-Br agrees with other imidazolium-based ILs [46] and quaternary ammonium ILs [31], which shows that the melting temperature decreases with the increase of the anion radius except for PF_6. This is attributed to the fact that ILs with PF_6 anions have stronger hydrogen bonds, owing to the F atom, and comparatively higher melting points. In the case of ammonium cations, the higher melting and decomposition temperatures may also be associated with the tetrahedral structure of ammonium cations and with the lack of any hydrogen bonds with the anion, which leads to the enhancement of Coulomb interaction and formation of ordered structures by the ions [31]. It has been suggested that the high thermal stability of hexafluorophosphates can be attributed to the fact that the decomposition of the salts is primarily determined by the decomposition of the cation [31]. However, the heat of fusion becomes larger when the ILs contain anions with larger negative charges [11]. Although the data presented in Table 1 lack the ultimate precision and accuracy achieved through calorimetry, they suggest that up to 2.5 wt % of the Al_2O_3 additive for TBA-Br and 5 wt % of the Al_2O_3 additive for TBA-PF_6 can potentially increase the heat of fusion, which is an important parameter in TES technology. At 10 wt % of the Al_2O_3 additive, the melting enthalpy values are lower than the corresponding values for pure ionic salts or other additive concentrations. This is in clear contrast to the results published by Bai et al. [25], who reported a very small variation for T_m and a monotonous decrease for ΔH_m with an additive concentration for an imidazolium-based IL and various copper and graphite additives that were separately added to an IL at a concentration of up to 25 wt %.

The effectiveness of the Al_2O_3 additive in TBA-Br and TBA-PF_6 ILs can be qualitatively explained as follows. Al_2O_3 is expected to dissolve in the larger IL component, i.e., undergoing strong interactions. At a certain amount of additive concentration, the dissolution of the additive may induce additional disorder in the system, as measured by the increase in entropy. From a thermodynamic perspective, it is related to the increase in the melting enthalpy at the same phase transition temperature. In the case of TBA-PF_6, a more complex mechanism may occur owing to the possibility for the decomposition scheme of TBA-PF_6 [31].

3. Materials and Methods

Tetrabutylammonium bromide (TBA-Br) also known as $[N^+{}_{4444}][Br^-]$ with the chemical formula $C_{16}H_{36}BrN$ (molecular weight, MW: 322 gr mol^{-1}) and tetrabutylammonium hexafluorophosphate (TBA-PF_6) also known as $[N^+{}_{4444}][PF_6{}^-]$ with the chemical formula $C_{16}H_{36}PF_6N$ (MW: 387 gr mol^{-1}) were acquired from Sigma Aldrich (2 Science Park Drive, Singapore) with a purity of 98%. Al_2O_3 nanoparticles (particle size < 50 nm) were also acquired from Sigma Aldrich. To investigate the additive effect on the physicochemical properties, Al_2O_3 was separately added to the TBA-PF_6 and TBA-Br ionic salts at various weight concentrations (2.5, 5, and 10 wt %), and the overall data were compared with pure TBA-Br and TBA-PF_6 samples. The mixed samples were obtained by thoroughly mixing an agate mortar for 5 min.

The Fourier transform infrared (IR) spectra of the samples were obtained by the IRPrestige21 spectrophotometer (Malang, East Java, Indonesia) from Shimadzu at a scanning number of 30 using the KBr sampling method. Simultaneous thermogravimetric analysis (TG) and differential thermal analysis (DTA) were performed using the LINSEIS STA PT1600 Platinum Series instrument (Malang, East Java, Indonesia) under an argon atmosphere (0.5 L min^{-1}). Samples between 5 and 15 mg were heated from 2 °C to 375 °C at a constant heating rate of 5 K min^{-1}. The data were further analyzed to obtain the differential scanning calorimetry (DSC) thermogram. We note that the low-temperature TG and DTA data of TBA-Br+Al_2O_3 ionic salts were eliminated owing to the water contribution, and the normalization was performed at 20 °C.

4. Conclusions

This paper describes the physical and thermal properties of TBA-Br and TBA-PF_6 added with Al_2O_3 concentrations of 0, 2.5, 5, and 10 wt % based on IR spectroscopy data and simultaneous TG, DTA, and DSC measurements. The IR spectra reveal the asymmetric/symmetric stretching and bending vibrations of the C–H, $–CH_2–$, and $–CH_3$ groups, which do not change with the addition of additive. The spectra also reveal the role of additive to the disappearance of the peaks at a lower wave number below 1000 cm^{-1} and the growth of a broad peak at 3500 cm^{-1}. The decomposition temperatures analyses show that TBA-Br remains stable with the addition of Al_2O_3. For TBA-PF_6, the dissolution of Al_2O_3 reduces the stability of the salt. In addition, the shift to a lower temperature of the high-temperature DTA peak signifies a chemical reaction between the additive and decomposition product of the salt. The melting temperatures of TBA-Br+Al_2O_3 salts are approximately constant (120 °C), whereas for TBA-PF_6+Al_2O_3, the melting temperature decreases from 248 to 213 °C and is relatively unchanged with increasing additive concentration. The total heat of fusion values strongly varied with the additive concentration, and the highest value was approximately 67 kJ kg^{-1} for the TBA-Br added with 2.5 wt % additive and the TBA-PF_6 added with 5 wt % additive. Compared to imidazolium-based ionic salts, certain concentrations of aluminium addition to these two ammonium-based ionic salts are more promising for TES.

Author Contributions: The experimental work was performed mainly by S.W. (Surjani Wonorahardjo); Visualisation by S.W. (Surjamanto Wonorahardjo); Funding acquisition was performed by I.M.S.; Both authors analysed the data and contributed to the preparation of the manuscript. All authors have read and agreed to the published version of the manuscript.

Funding: This research was funded by the ASAHI-2018 research project, grant number 3215/I1.B04.1/PL/2018.

Acknowledgments: We thank to Nandang Mufti for TG-DTA/DSC measurements. We would like to thank Editage (www.editage.com) for English language editing.

Conflicts of Interest: The authors declare no conflict of interest.

References

1. Rooney, D.; Jacquemin, J.; Gardas, R. Thermophysical Properties of Ionic Liquids. In *Ionic Liquids*; Kirchner, B., Ed.; Springer: Berlin/Heidelberg, Germany, 2009; pp. 185–212.
2. MacFarlane, D.R.; Kar, M.; Pringle, J.M. *Fundamentals of Ionic Liquids, From Chemistry to Applications*; Wiley: Weinheim, Germany, 2017.
3. Mallakpour, S.; Dinari, M. Ionic Liquids as Green Solvents: Progress and Prospects. In *Green Solvents II Properties and Application of Ionic Liquids*; Mohammad, A., Inamuddin, D., Eds.; Springer: Dordrecht, The Netherlands, 2012; pp. 1–32.
4. Wu, B.; Reddy, R.G.; Rogers, R.D. *Novel ionic liquid thermal storage for solar thermal electric power systems In Proceedings, Solar Forum 2001 Solar Energy*; The Power to Choose: Washington, DC, USA, 2001; pp. 445–451.
5. Valkenburg, M.E.V.; Vaughn, R.L.; Williams, M.; Wilkes, J.S. Thermochemistry of ionic liquid heat-transfer fluids. *Thermochim. Acta* **2005**, *425*, 181–188. [CrossRef]
6. Masayoshi, W.; Morgan, L.T.; Shiguo, Z.; Kazuhide, U.; Tomohiro, Y.; Kaoru, D. Application of Ionic Liquids to Energy Storage and Conversion Materials and Devices. *Chem. Rev.* **2017**, *117*, 7190–7239. [CrossRef]
7. Fan, L.; Kang, S.; Wu, J.; Hao, S.; Lan, Z.; Lin, J. Quasi-Solid State Dye-sensitized Solar Cells Based on Polyvinylpyrrolidone With Ionic Liquid. *Energy Sources A* **2010**, *32*, 1559–1568. [CrossRef]
8. Devaki, S.J.; Sasi, R. Ionic Liquids/Ionic Liquid Crystals for Safe and Sustainable Energy Storage Systems. In *Progress and Developments in Ionic Liquids*; Handy, S., Ed.; Intech Europe: Rijeka, Croatia, 2017; pp. 313–336. [CrossRef]
9. Burns, J.A.; Verrall, R.E. Thermodynamics of tetraalkyl- and bis-tetraalkylammonium bromides: II. Heat capacities of solid state from 273 to 373 K. *Thermochim. Acta* **1974**, *9*, 277–288. [CrossRef]
10. Zhu, J.; Bai, L.; Chen, B.; Fei, W. Thermodynamical properties of phase change materials based on ionic liquids. *Chem. Eng. J.* **2009**, *147*, 58–62. [CrossRef]

11. Zhang, Z.; Salih, A.A.M.; Li, M.; Yang, B. Synthesis and Characterization of Functionalized Ionic Liquids for Thermal Storage. *Energy Fuels* **2014**, *28*, 2802–2810. [CrossRef]
12. Fukushima, T.; Aida, T. Ionic liquids for soft functional materials with carbon nanotubes. *Chem. Eur. J.* **2007**, *13*, 5048–5058. [CrossRef]
13. Nieto de Castro, C.A.; Lourenço, M.J.V.; Ribeiro, A.P.C.; Langa, E.; Vieira, S.I.C.; Goodrich, P.; Hardacre, C. Thermal properties of ionic liquids and ionanofluids of imidazolium and pyrrolidinium liquids. *J. Chem. Eng. Data* **2010**, *55*, 653–661. [CrossRef]
14. Ribeiro, A.P.C.; Vieira, S.I.C.; França, J.M.; Queirós, C.S.; Langa, E.; Lourenço, M.J.V.; Murshed, S.M.S.; Nieto de Castro, C.A. Thermal Properties of Ionic Liquids and Ionanofluids. In *Ionic Liquids: Theory, Properties, New Approaches*; Kokorin, A., Ed.; Intech Europe: Rijeka, Croatia, 2011; pp. 37–60. [CrossRef]
15. Murshed, S.M.S.; Nieto de Castro, C.A.; Lourenço, M.J.V.; França, J.; Ribeiro, A.P.C.; Vieira, S.I.C.; Queirós, C.S. Ionanofluids as Novel Fluids for Advanced Heat Transfer Applications, World Academy of Science. *Int. J. Math. Comput. Phys. Electr. Comput. Eng.* **2011**, *5*, 795–798.
16. Liu, J.; Wang, F.; Zhang, L.; Fang, X.; Zhang, Z. Thermodynamic properties and thermal stability of ionic liquid-based nanofluids containing graphene as advanced heat transfer fluids for medium-to-high-temperature applications. *Renew. Energy* **2014**, *63*, 519–523. [CrossRef]
17. Wang, B.; Wang, X.; Lou, W.; Hao, J. Rheological and tribological properties of ionic liquid-based nanofluids containing functionalized multi-walled carbon nanotubes. *J. Phys. Chem. C* **2010**, *114*, 8749–8754. [CrossRef]
18. Wang, B.; Wang, X.; Lou, W.; Hao, J. Ionic liquid-based stable nanofluids containing gold nanoparticles. *J. Colloid Interface Sci.* **2011**, *362*, 5–14. [CrossRef] [PubMed]
19. Jwo, C.S.; Change, H.; Teng, T.P.; Kao, M.J.; Guo, Y.T. A study on the effects of temperature and volume fraction on thermal conductivity of copper oxide nanofluid. *J. Nanosci. Nanotechnol.* **2007**, *7*, 2161–2166. [CrossRef] [PubMed]
20. Cheng, L.J.; Guo, L.J. Ionic current rectification, breakdown, and switching in heterogeneous oxide nanofluidic devices. *ACS Nano* **2009**, *3*, 575–584. [CrossRef]
21. Chang, H.; Kao, M.J.; Chang, Y.C.; Huang, D.Y. A new approach of synthesis of Al_2O_3 nanofluid. In Proceedings of the 3rd Workshop on Metastable and Nanostructured Materials, NANOMAT, Rio de Janeiro, Brazil, 5–8 June 2006; Trans Tech Publications Ltd.: Freienbach, Switzerland, 2008; pp. 155–161.
22. Titan, C.P.; Morshed, A.K.M.M.; Fox, E.B.; Visser, A.E.; Bridges, N.J.; Khan, J.A. Enhanced Thermal Performance of Ionic Liquid-Al_2O_3 Nanofluid as Heat Transfer Fluid for Solar Collector. In Proceedings of the ASME 7th International Conference on Energy Sustainability, ES-FuelCell2013, Minneapolis, MN, USA, 14–19 July 2013.
23. Zhang, L.; Liu, J.; He, G.; Ye, Z.; Fang, X.; Zhang, Z. Radiative properties of ionic liquid-based nanofluids for medium-to-high-temperature direct absorption solar collectors. *Sol. Energy Mater. Sol. Cells* **2014**, *130*, 521–528. [CrossRef]
24. Bridges, N.J.; Visser, A.E.; Fox, E.B. Potential of Nanoparticle-Enhanced Ionic Liquids (NEILs) as Advanced Heat-Transfer Fluids. *Energy Fuels* **2011**, *25*, 4862–4864. [CrossRef]
25. Bai, L.; Li, X.; Zhu, J.; Chen, B. Effects of Nucleators on the Thermodynamic Properties of Seasonal Energy Storage Materials Based on Ionic Liquids. *Energy Fuels* **2011**, *25*, 1811–1816. [CrossRef]
26. Mineaa, A.A.; Murshed, S.S. A review on development of ionic liquid based nanofluids and their heat transfer behaviour. *Renew. Sustain. Energy Rev.* **2018**, *91*, 584–599. [CrossRef]
27. Bhatt, V.D.; Gohil, K. Performance evaluation of solar cooker using some [N^+_{4444}] based ionic liquids as thermal energy storage materials. *Adv. Mater. Lett.* **2013**, *4*, 277–282. [CrossRef]
28. Fifield, F.W.; Kealey, D. *Principles and Practice of Analytical Chemistry*, 5th ed.; Blackwell Science Ltd.: Cambridge, UK, 2000; ISBN 0-632-05384-4.
29. Wang, Q.; Habenschuss, A.; Xenopoulos, A.; Wunderlich, B. Mesophases of Alkylammonium Salts. VI. The Crystal Structures of Tetra-nbutylammonium Bromide and Iodide. *Mol. Cryst. Liq. Cryst.* **1995**, *264*, 115–129. [CrossRef]
30. Xenopoulos, A.; Cheng, J.; Yasuniwat, M.; Wunderlich, B. Mesophases of Alkylammonium Salts. I. First-Order Transitions. *Mol. Cryst. Liq. Cryst.* **1992**, *214*, 63–79. [CrossRef]
31. Zhuravlev, O.E.; Nikol'skii, V.M.; Voronchikhina, L.I. Thermal Stability of Quaternary Ammonium Hexafluorophosphates and Halides. *Russ. J. Appl. Chem.* **2013**, *86*, 824–830. [CrossRef]

32. Blundell, R.K.; Licence, P. Quaternary ammonium and phosphonium based ionic liquids: A comparison of common anions. *Phys. Chem. Chem. Phys.* **2014**, *16*, 15278–15288. [CrossRef]
33. Lassègues, J.C.; Grondin, J.; Cavagnat, D.; Johansson, P. New Interpretation of the CH Stretching Vibrations in Imidazolium-Based Ionic Liquids. *J. Phys. Chem. A* **2009**, *113*, 6419–6421. [CrossRef] [PubMed]
34. Wulf, A.; Fumino, K.; Ludwig, R. Comment on "New Interpretation of the CH Stretching Vibrations in Imidazolium-Based Ionic Liquids". *J. Phys. Chem. A* **2010**, *114*, 685–686. [CrossRef]
35. Lassegues, J.C.; Grondin, J.; Cavagnat, D.; Johansson, P. Reply to the "Comment on 'New Interpretation of the CH stretching Vibrations in Imidazolium-Based Ionic Liquids'". *J. Phys. Chem. A* **2010**, *114*, 687–688. [CrossRef]
36. Harmon, K.M.; De Santis, N.J.; Brandt, D.O. Hydrogen bonding Part 39. Hydrogen bonding by α-CH in quaternary ammonium salts and the possible role of CHB hydrogen bonds in acetylcholine—Receptor interactions. *J. Mol. Struct.* **1992**, *265*, 47–57. [CrossRef]
37. Coates, J. Interpretation of Infrared Spectra, a Practical Approach. In *Encyclopedia of Analytical Chemistry*; Meyers, R.A., Ed.; John Wiley and Sons Ltd.: Chichester, UK, 2000; pp. 10815–10837.
38. Paschoal, V.H.; Faria, L.F.O.; Ribeiro, M.C.C. Vibrational Spectroscopy of Ionic Liquids. *Chem. Rev.* **2017**, *117*, 7053–7112. [CrossRef]
39. Falk, M.; Ford, T.A. Infrared spectrum and structure of liquid water. *Can. J. Chem.* **1966**, *44*, 1699–1707. [CrossRef]
40. Ates, M.; Demir, V.; Arslan, Z.; Daniels, J.; Farah, I.O.; Bogatu, C. Evaluation of Alpha and Gamma Aluminum Oxide Nanoparticle Accumulation, Toxicity and Depuration in *Artemia Salina* Larvae. *Environ. Toxicol.* **2015**, *30*, 109–118. [CrossRef]
41. Richter, J.; Ruck, M. Synthesis and Dissolution of Metal Oxides in Ionic Liquids and Deep Eutectic Solvents. *Molecules* **2020**, *25*, 78. [CrossRef]
42. Wang, Z.; Huang, X.; Chen, L. Understanding of Effects of Nano-Al_2O_3 Particles on Ionic Conductivity of Composite Polymer Electrolytes. *Electrochem. Solid St (ESL)* **2003**, *6*, E40–E44. [CrossRef]
43. Lü, R.; Lin, J.; Lu, Y.; Liu, D. The comparison of cation–anion interactions of phosphonium- and ammonium-based ionic liquids—A theoretical investigation. *Chem. Phys. Lett.* **2014**, *597*, 114–120. [CrossRef]
44. Erdmenger, T.; Vitz, J.; Wiesbrock, F.; Schubert, U.S. Influence of different branched alkyl side chains on the properties of imidazolium-based ionic liquids. *J. Mater. Chem.* **2008**, *18*, 5267–5273. [CrossRef]
45. Golding, J.; Forsyth, S.; MacFarlane, D.R.; Forsyth, M.; Deacon, G.B. Methanesulfonate and *p*-toluenesulfonate salts of the *N*-methyl-*N*-alkylpyrrolidinium and quaternary ammonium cations: Novel low cost ionic liquids. *Green Chem.* **2002**, *4*, 223–229. [CrossRef]
46. Zhang, S.; Sun, N.; He, X.; Lu, X.; Zhang, X. Physical Properties of Ionic Liquids: Database and Evaluation. *J. Phys. Chem. Ref. Data* **2006**, *35*, 1475–1517. [CrossRef]



© 2020 by the authors. Licensee MDPI, Basel, Switzerland. This article is an open access article distributed under the terms and conditions of the Creative Commons Attribution (CC BY) license (http://creativecommons.org/licenses/by/4.0/).